



# Phase formation and mechanical properties of iron-based intermetallic/steel laminate composites

Yu Wang<sup>1,2</sup> · Yaxin Liu<sup>1</sup> · Hongyang Pan<sup>1</sup> · Jibo Hou<sup>1</sup> · Hongkui Mao<sup>1</sup> · Bin Liu<sup>1</sup> · Hong Xu<sup>1</sup> · Peikang Bai<sup>1</sup> · R. D. K. Misra<sup>3</sup>

Received: 26 February 2021 / Revised: 28 April 2021 / Accepted: 30 April 2021 / Published online: 14 June 2021  
© The Author(s), under exclusive licence to Springer Nature Switzerland AG 2021

## Abstract

In the present study, the relationship between microstructure and mechanical properties of steel-based intermetallic-metal-laminated composites processed via diffusional reaction is clarified. Steel and pure Al foils were alternately stacked and isothermally heated in vacuum at 655 °C for 2–16 h and subjected to a pressure of 3.8 MPa ultimately leading to laminate composite. The phase formation sequence and mechanical properties of the steel/FeAl intermetallic-laminated composite was firstly studied using different characterization techniques. The intermetallics formed in the laminated composite were Fe<sub>2</sub>Al<sub>5</sub> and FeAl phase, whose growth governed was the kinetics of diffusion. The microhardness distribution of the steel-based MIL is consistent with the goal of combining high strength and stiffness of the intermetallic phase (1000 HV) with high toughness and ductility of the metal (100 HV). The compressive strength of laminated composites was 950 MPa. With the formation of FeAl phase between steel and brittle Fe<sub>2</sub>Al<sub>5</sub>, two peaks present in the stress-strain curve with the strain increase; the fracture morphology was characterized by a combination of ductile and brittle fracture.

**Keywords** Metal intermetallic laminate composites · Diffusional reaction · Phase transformation · Mechanical properties

## 1 Introduction

Processing of laminated composites is an effective method to exploit the properties of individual bulk materials [1, 2]. The strength of intermetallics is good, but the room temperature brittleness limits its use as structural materials. The toughness of intermetallics can be enhanced via particles [3], fibers, or layers of ductile metals [4] to compensate for the limited room temperature deformation and to inhibit crack growth. Among them, the laminated structure has superior reinforcement effect [5, 6]. The hybrid-laminated structure referred as metal-intermetallic-laminated (MIL) composites can be effectively designed to optimize the

unique properties and exploit the benefits of the individual constituents by incorporating high strength and stiffness of the intermetallic phase with high toughness of the metallic constituent [7]. The appropriate MIL microstructure can be obtained by designing and optimizing the nature of initial foil, thickness, the number of layers of each constituent, and the process. MIL composites are generally characterized by excellent mechanical properties such as high strength, high stiffness, fracture toughness, wear resistance, and low cost [7–9]. Meanwhile, compared with methods such as rolling and explosive welding, the bonding interface formed by hot pressing of present study has stronger metallurgical interface and does not cause environmental pollution. Therefore, MIL laminate composites can be used as high-temperature structural materials and in applications that require high energy absorption [5, 10].

MIL composite systems of Ti/Al [11–13] and Fe/Al [14–16] system have been widely studied. The evolution of the intermetallic phase in the microstructure was studied by Vecchio [7] and Azimi et al. [14] and the fracture behavior was in detail by Rohatgi et al. [5, 13] and Brunelli et al. [16]. The unique mechanical properties of Ti-Al<sub>3</sub>Ti MIL composites were shown to be derived from the hierarchical structure

✉ Yu Wang  
wangyu@nuc.edu.cn

<sup>1</sup> School of Materials Science and Engineering, North University of China, Taiyuan 030051, China

<sup>2</sup> Anhui Hengli Additive Manufacturing Technology Co., Ltd, Wuhu 241200, China

<sup>3</sup> Department of Metallurgical, Materials and Biomedical Engineering, University of Texas at El Paso, El Paso, TX 79968, USA

**Table 1** Chemical composition of carbon steel (wt%)

Element	C	Si	Mn	S	P	Fe
Content	0.14–0.22	0.3	0.30–0.65	≤0.05	≤0.045	Balance

of laminates and the significant degree of toughening was achieved with a small volume fraction of remnant metal layers. Thus, it is desirable to fabricate similar MIL composites from lower cost sheet metals, specifically replacement of Ti with Fe-based sheet metal. Stainless steels (430SS and 304SS) were used in place of Ti-based materials to prepare MIL composites with the aim to have mechanical properties comparable to Ti-Al<sub>3</sub>Ti composites. Microstructural studies on stainless steel-based MIL composites revealed that brittle Al-rich intermetallic Fe<sub>2</sub>Al<sub>5</sub> formed in the intermetallic layer increases the stress concentration at the intermetallic/metal interface causing cracking or delamination [17]. The abrupt change of hardness between brittle aluminum-rich phase and flexible metal layer is the main reason for stress concentration and delamination at the interface of laminated materials [17].

The Fe-rich intermetallic compounds (FeAl and Fe<sub>3</sub>Al) have proven to exhibit coherent interface with iron-based alloy with higher toughness than the Al-rich intermetallics. The strength and hardness of Fe-rich intermetallic compounds are slightly lower than Al-rich phases. They exhibit good plasticity and toughness because of more number of slip systems. Therefore, the formation of iron-rich phase (FeAl) at the intermetallic/metal interface can reduce the atomic mismatch at the interface, change the abrupt hardness decrease between the intermetallic layer and the metal layer, and relieve the stress concentration at the interface [18, 19]. It is desirable to obtain relatively ductile intermetallics with as much iron content as possible (FeAl<sub>2</sub>, FeAl, and Fe<sub>3</sub>Al) between the the Fe<sub>2</sub>Al<sub>5</sub>/Fe interface to decrease the stress concentration. While the presence of 17 at.% Cr in the stainless steel acts as a barrier in the diffusional reaction system suppressing the phase transformation from Fe-rich intermetallic between Al and Fe by forming two types of chromium-aluminum intermetallic phases Cr<sub>2</sub>Al<sub>13</sub> and Al<sub>10</sub>Cr<sub>5.5</sub>Fe<sub>2.5</sub>. Hence, steel without Cr or Ni elements has a reduced tendency to form aluminide via reaction of Cr with Al. It is a viable approach to potentially obtain Fe-rich compound with good toughness by using steel reacted with aluminum.

Previous studies focused on the interaction between Al and steel [20–22] have shown that the common Fe<sub>2</sub>Al<sub>5</sub>

phases were nucleated on the surface of carbon steel, when steel was hot-dipping into a molten aluminum bath at 700 °C and annealing at 750 °C in static air. The increase of exposure time in air led to the disappearance of Fe<sub>2</sub>Al<sub>5</sub> phase which was gradually replaced by FeAl phase [21]. In another study, steel was plasma pack aluminized at 700 °C in vacuum at 15 mbar, followed by oxidation at 800 °C temperature for 1 h. The results showed that besides FeAl<sub>3</sub> and Fe<sub>2</sub>Al<sub>5</sub> phases, Fe<sub>3</sub>Al and FeAl intermetallic were also observed [22] on extended annealing treatment at elevated temperature.

In the present study, steel-based MIL composites were processed via diffusional reaction (at 655 °C) for different times to obtain Fe-rich intermetallic phases (FeAl phase). The microstructure evolution and growth kinetics of intermetallic layers were studied and related to mechanical properties together with the study of micro-hardness distribution across the intermetallic/metal interface and evaluation of static compression performance. The objective of the study is to elucidate the effect of microstructure of intermetallics formed at the interface of carbon steel/Al on mechanical properties of MIL composites.

## 2 Experimental

### 2.1 Materials

The materials used for fabricating the laminates were steel and 1060 Al foils of chemical composition listed in Tables 1 and 2, respectively. Both carbon steel and 1060 Al were commercially available metal foil strips of dimensions 20 mm × 40 mm × 0.2 mm.

### 2.2 Processing of laminated composite

1060 Al foils were etched with 9% NaOH solution for 5 min, while steel was not subjected to etching. The metal foils were ground with 240 grit coarse SiC paper and cut to dimensions of 20 mm × 20 mm × 0.2 mm. Ground foils were ultrasonically cleaned for 10 min with ethanol and dried by cold air. Vacuum hot pressing furnace

**Table 2** Chemical composition of 1060 Al (wt%)

Element	Si	Fe	Cu	Mg	Mn	Zn	Ti	V	Al
Content	0.25	0.35	0.05	0.03	0.03	0.05	0.03	0.05	Balance

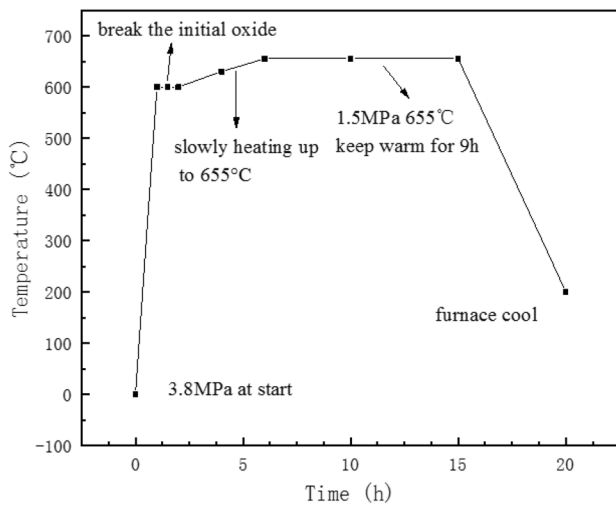
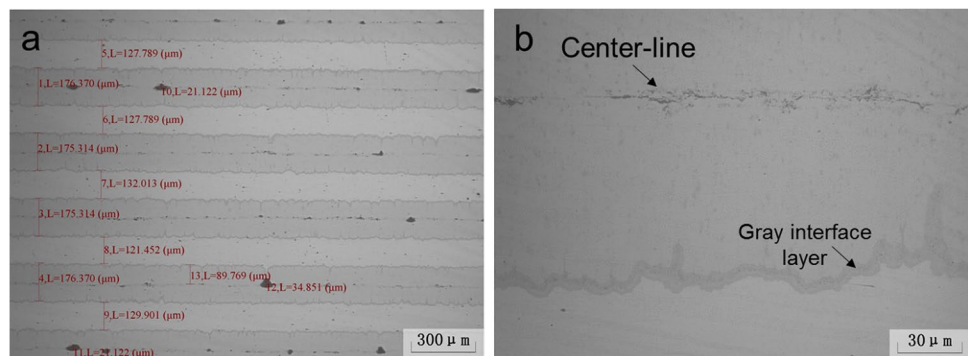


**Fig. 1** The heating temperature and time curve for the laminated composite

(OTF-1200X) manufactured by Hefei Kejing Material Technology Ltd. was used. The pre-processed carbon steel and Al foils were stacked alternately (18 layers of carbon steel, 17 layers of Al) and placed in a graphite mold. Next, the mold with the sample was placed between the upper and lower graphite pressure bars of the hot pressing furnace and hot pressing of MIL composites accomplished.

After the sample was placed in a vacuum hot pressing furnace, the pressure of the sample was set to 3.8 MPa and evacuated to  $1 \times 10^{-1}$  Pa. The heating temperature and time curve are shown in Fig. 1. The temperature was increased from room temperature to 600 °C at a heating rate of 10 °C/min. The sample was heated at 600 °C for a certain period of time to break the initial oxide layer and start the diffusion of iron and aluminum. After slowly heating up to 655 °C, it is kept warm for a period of time and then finally cooled inside the furnace. The microstructural evolution associated with the reaction of carbon steel with Al after reaction was studied for samples kept for 2, 4, 6, 8, 12, and 16 h at constant temperature.

**Fig. 2** An image of carbon steel/Al heated at 655 °C for 2 h



## 2.3 Microstructure evolution and characterization

The prepared samples were cut in the direction perpendicular to the reaction interface to obtain cross-section. Cross-section of the samples was first ground with a series of SiC paper (240–2000 grit) and then mechanically polished with diamond paste using standard metallographic procedure. The microstructure of the cross-section was observed with Leica MEF-4 optical microscope and Hitachi SU5000 field emission SEM. EDS EBSD and XRD techniques were used to study chemical analysis and phases, respectively.

The following methods were used to measure density. The mass of each sample was measured by a scale with a hook at the bottom with an accuracy of 0.001 g, and then, the sample was tied with a fine wire of a certain length. The remaining fine line ends were fixed, the samples were weighed successively in air and distilled water, and the density of the samples was calculated. The actual density was calculated and compared with the theoretical density value calculated in Sect. 3.2 below. The micro-hardness of the MIL composites was measured at an indentation load of 0.2 kg for 10 s using a Shanghai Siwei HVS-1000 micro-hardness tester. The quasi-static compression test was performed using a WE-30 microcomputer-controlled electro-hydraulic servo universal material testing machine. A cylindrical sample having a diameter of 5 mm was processed by a wire cutting method. The loading direction was perpendicular to the lamination direction and the strain rate was 0.001 mm/s. After the test, the fracture morphology of the sample was observed by SEM.

## 3 Results

### 3.1 Microstructure

Figure 2 shows the image of steel-based MIL composite after 2 h of treatment. It can be seen from Fig. 2 that a uniform interlayer was obtained by hot-pressure diffusion, which is called uniform layer. Al was not completely

consumed and reacted with Fe in carbon steel to form an intermetallic layer with tongue-like morphology. When Fe and Al diffused, the intermetallic grew on both sides, forming a tongue-like uneven interface on the near carbon steel side. At the same time, impurity oxides were present in the intermediate region, forming the “intermetallic centerline”. In addition, it was observed that there was a thin layer of gray scale between the intermetallic compound layer and the carbon steel, which is believed to be another intermetallic compound [23].

The results of EDS scan of the sample are shown in Fig. 3. Blue represents Al and green represents Fe. From the color distribution, the thicker layer on the right side and the thinner layer in the middle are both Fe-Al intermetallics. In order to understand the phase composition of the two Fe-Al intermetallics, EDS analysis was carried out from the Fe-rich side to the Al-rich side in the direction perpendicular to the interface. The line scan result suggested that the distribution of Al and Fe was relatively uniform, and a two-stage platform appeared. The average atomic content (Al: 68.2 at% and Fe: 31.8 at%) in the main intermetallic layer (left part of the EDS line scan) indicated that the formed phase is  $\text{Fe}_2\text{Al}_5$

phase, which is the most thermodynamically stable phase in the Al-Fe system and is the first phase formed during Al-Fe interaction. EDS analysis results around the interface area (Al: 56.7 at% and Fe: 43.3 at%) indicated that high iron content intermetallic phases are formed at the interface area between  $\text{Fe}_2\text{Al}_5$  and Fe.

To further determine the phase composition of Fe-Al intermetallic compounds, XRD analysis was performed, as shown in Fig. 4. Phase identification was performed by XRD detection. The diffraction peak of FeAl phase was also observed, together with the diffraction peaks of (110) crystal planes of elemental steel and file of  $\text{Fe}_2\text{Al}_5$  with the first and second peaks at  $44.55^\circ$  and  $43.78^\circ$ , respectively.

### 3.2 Density

In order to study the compactness of steel-based MIL composites by hot pressing, the microstructure was observed, and the theoretical density of the materials was calculated. Images for different heating time are presented in Fig. 5.

According to the structural characteristics of the samples shown in Fig. 6, the theoretical density of MIL composites is

**Fig. 3** Cross-sectional EDS spot and line scan analysis of carbon steel/Al reaction

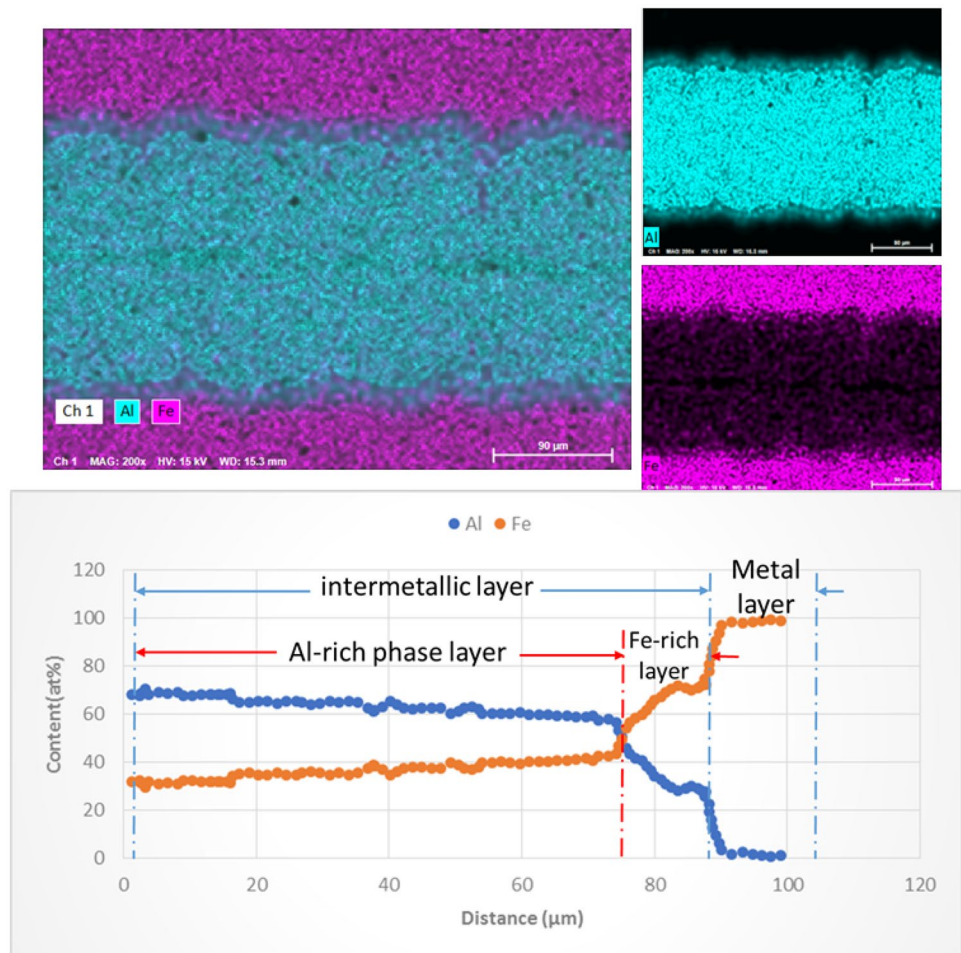
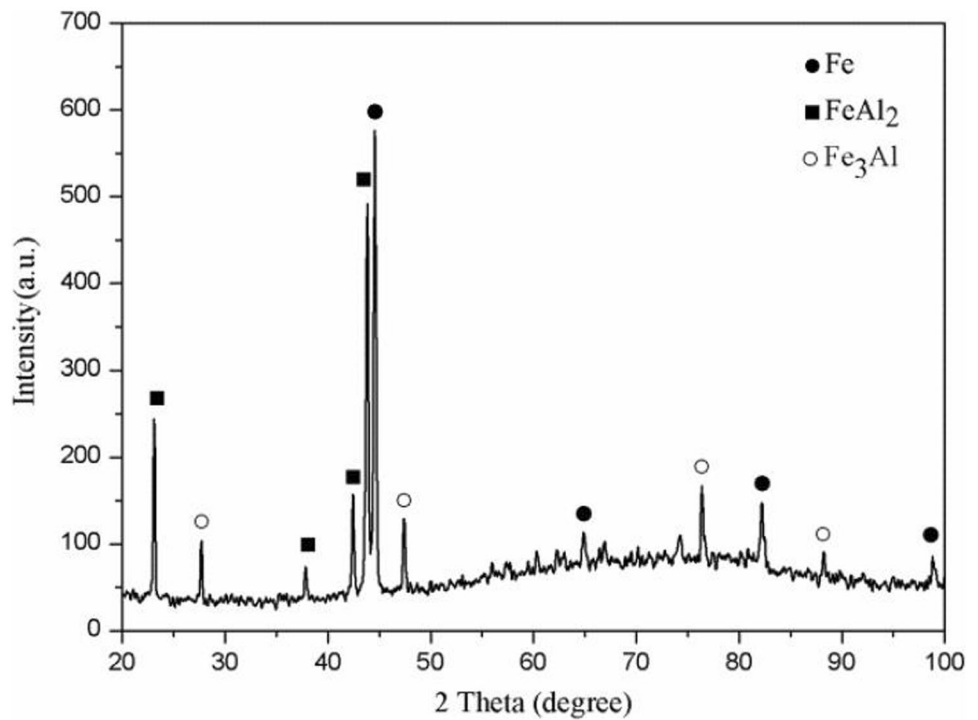


**Fig. 4** XRD of carbon steel/Al heated at 655 °C for 4 h



$$\rho_T = \frac{m_T}{V_T} = \frac{\sum_{i=1}^3 \rho_i \times ab \times n_i \delta_i}{\sum_{i=1}^3 ab \times n_i \delta_i} = \frac{\sum_{i=1}^3 \rho_i \times n_i \delta_i}{\sum_{i=1}^3 n_i \delta_i} \quad (1)$$

where  $\rho_T$  is the theoretical density of MIL composite and the unit is  $\text{g/cm}^3$ .  $m_T$  is mass and its unit is g.  $V_T$  is volume and its unit is  $\text{cm}^3$ .  $i = 1, 2, 3$  represents  $\text{Fe}_2\text{Al}_5$ , FeAl, and carbon steel, respectively.  $a$  and  $b$  are the length and width perpendicular to the laminated interface, respectively. For the determination of length and width of each layer, the length is equivalent for all  $\text{Fe}_2\text{Al}_5$  layers at each cross section after the oxidation layer is broken. The contrast between compound /Fe and compound/oxide interfaces is clearly discernible. Therefore, the length and width of  $\text{Fe}_2\text{Al}_5$  layers can be obtained by using the capture boundary function of Photoshop.  $\rho_i$ ,  $\delta_i$ , and  $n_i$  indicate the density, the thickness, and the number of layers of each phase, respectively. All length units are  $\mu\text{m}$ . The actual density of carbon steel is  $7.85 \text{ g/cm}^3$ , the theoretical density of  $\text{Fe}_2\text{Al}_5$  is  $4.46 \text{ g/cm}^3$ , and FeAl is  $5.56 \text{ g/cm}^3$ , respectively [23]. The carbon steel and Al used in the experiment had 18 and 17 layers, respectively, and considering the binary phase diagram of Fe–Al, it was found that  $n_1 = 17$ ,  $n_2 = 34$ , and  $n_3 = 18$ , respectively,  $\delta_1$  and  $\delta_3$  are thickness at different time.

Since the shape of the sample after cutting and grinding is not regular, the actual volume was measured as using the method described in Sect. 2.3. The actual mass was measured by an electronic balance. For samples with different heating times, the actual density is calculated by

$$\rho_c = \frac{\rho_{\text{water}} m_a}{m_a - m_{\text{water}}} \quad (2)$$

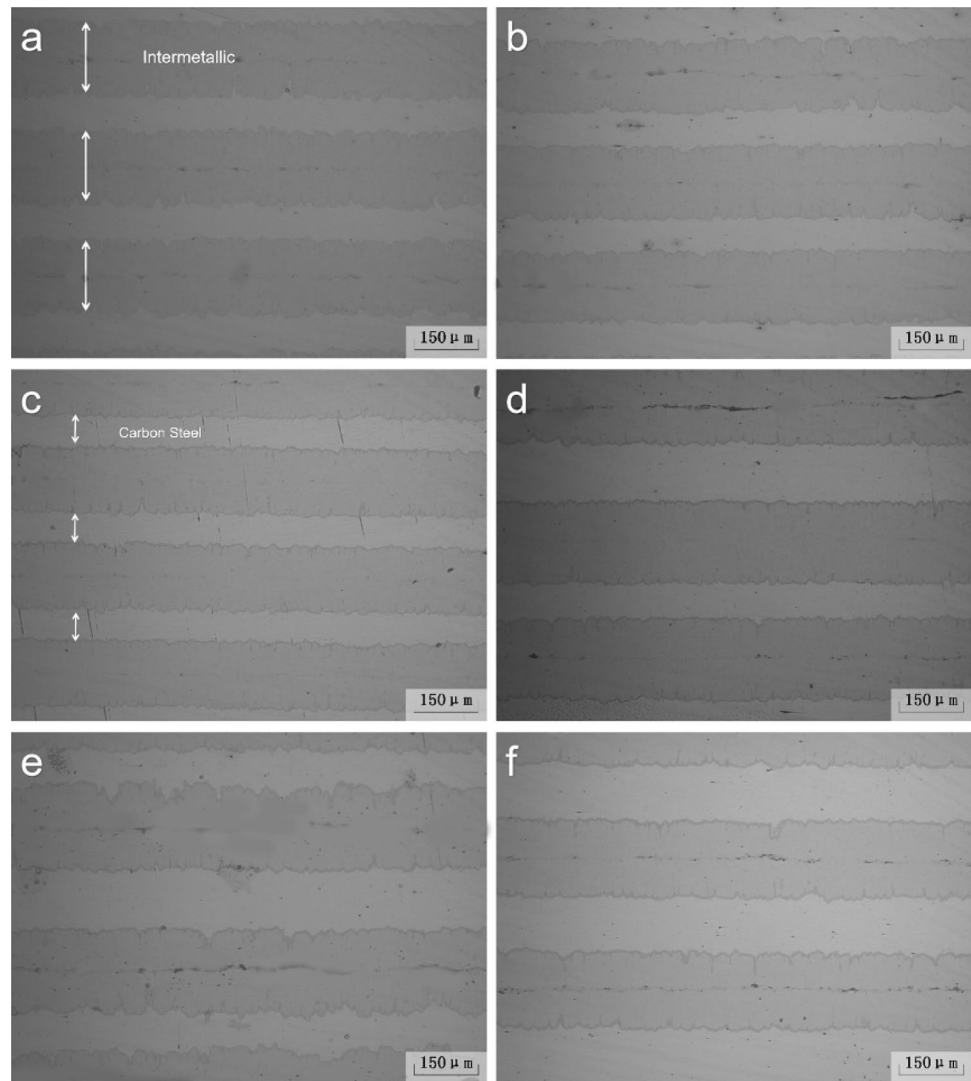
The theoretical density and the calculated density are shown in Table 3.

The density map of each time period was drawn and is shown in Fig. 6. The picture notes that during the 2 h reaction time of incomplete Al reaction, the calculated density was reduced due to the formation of  $\text{Fe}_2\text{Al}_5$ . The metallographic images of a, b, c, d were for 6 h, 8 h, 12 h, and 16 h, respectively. After complete reaction of Al, with the extension of time, further diffusion occurred and  $\text{Fe}_2\text{Al}_5$  transformed to FeAl phase and the thickness increased with time, as shown in the Fig. 6a–d. Therefore, the calculated density in the subsequent reaction time was lower than the theoretical density. In order to investigate the growth of intermetallic compounds, the growth kinetics were investigated (Fig. 7).

### 3.3 Kinetics

As described above, at 655 °C, a thick  $\text{Fe}_2\text{Al}_5$  layer and a very thin FeAl layer were formed at the carbon steel/Al interface, and Al was completely consumed. According to the binary phase diagram of Fe–Al [24], stable Fe–Al intermetallics are FeAl,  $\text{FeAl}_2$ ,  $\text{Fe}_2\text{Al}_5$ , and  $\text{FeAl}_3$  phases at 655 °C. However, according to above,  $\text{Fe}_2\text{Al}_5$  phase and a thin FeAl layer were present. It is not certain that all the stable phases can be formed while some of them cannot grow into a visible layer after a long period of heating. In

**Fig. 5** Images of carbon steel/Al heated at 655 °C for different time (**a** 2 h, **b** 4 h, **c** 6 h, **d** 8 h, **e** 12 h, **f** 16 h)



order to understand the specific reaction diffusion mechanism of the two intermetallics, it is necessary to study the growth kinetics (Table 4).

From Fig. 3, the thickness of  $\text{Fe}_2\text{Al}_5$  and  $\text{FeAl}$  layers can be calculated from [25]

$$l_i = \frac{A_i}{w} \quad (3)$$

where the area, length, and thickness of the intermetallic layer are  $A_i$ ,  $w$ , and  $l_i$ , respectively. The unit of length is  $\mu\text{m}$  and  $w$  of each intermetallic layer is obtained from the cross section.  $\text{Fe}_2\text{Al}_5$ ,  $\text{FeAl}$ , and carbon steel have different gray-level scale, or contrast. Thus, the interface corresponding to  $\text{Fe}_2\text{Al}_5$  and  $\text{FeAl}$  can be distinguished clearly. The  $\text{Fe}_2\text{Al}_5$  and  $\text{FeAl}$  layers are defined  $i = 1, 2$ , respectively.

The basic empirical formula for the growth of intermetallics [25] is given by

$$l_i = k \left( \frac{t}{t_0} \right)^n \quad (4)$$

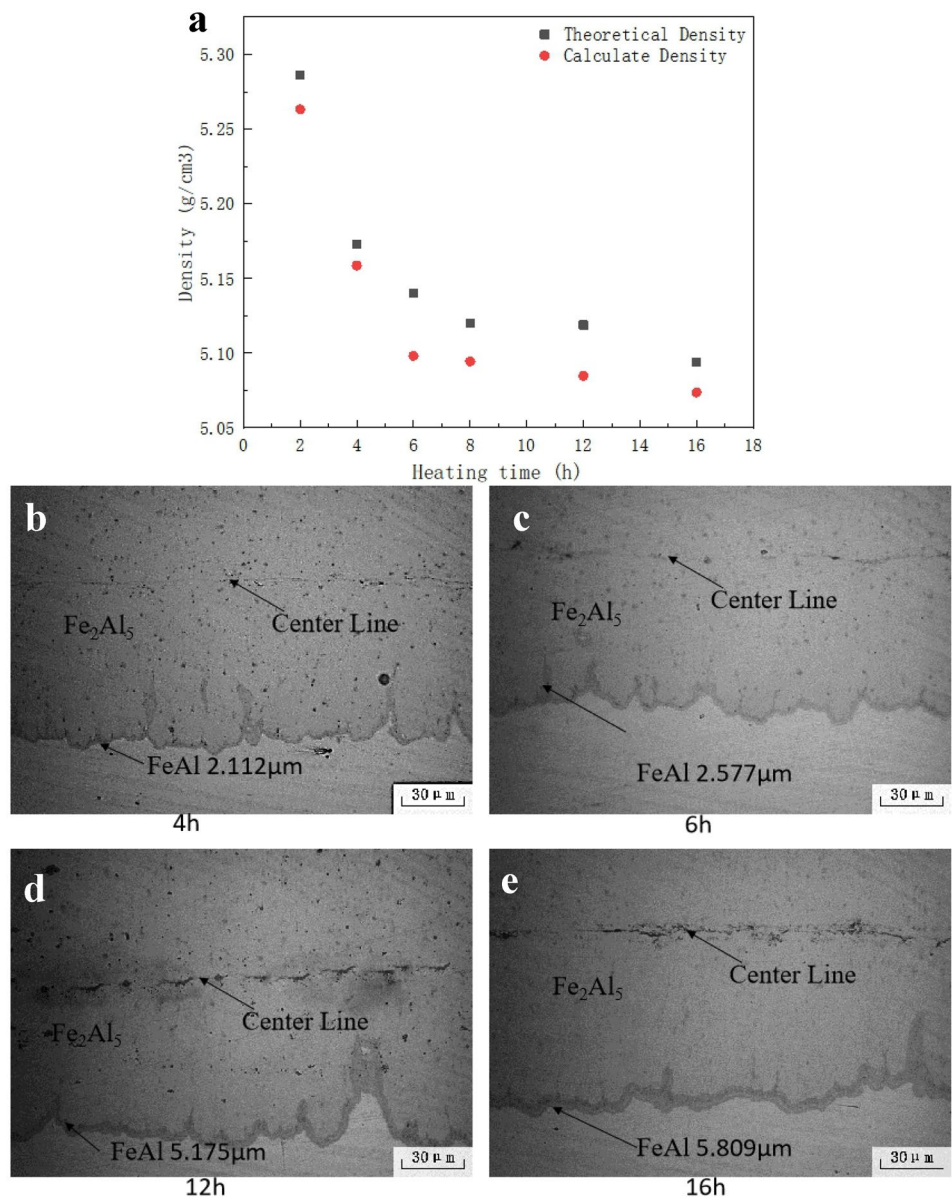
where  $t$  and  $t_0$  are the heating time and the unit time, respectively. Time unit is  $h$  and  $t/t_0$  is dimensionless. The proportional coefficient  $k$  is the same dimension as  $l_i$ , so its unit is also  $\mu\text{m}$ .

Taking logarithm on both sides of Eq. (4), get that:

$$\ln l_i = n \ln \frac{t}{t_0} + \ln k \quad (5)$$

where the relationship between the thickness of intermetallic layer is fitted according to the Eq. (5), and the curve of

**Fig. 6** Density distribution of different heating time (a) and the corresponding microstructure (b 4h, c 6h, d 12h, e 16h)



$l_i - \ln \frac{l}{l_0}$  is shown in Fig. 7. The fitted equation is shown in Table 4. It can be seen that the index obtained by fitting is close to 0.5, which indicates that the thicknesses of  $Fe_2Al_5$  and FeAl phases are both proportional to the square root of the heating time. That is the growth of  $Fe_2Al_5$  and FeAl phases is controlled by volume diffusion.

### 3.4 Microhardness

The reaction-generated intermetallic compounds were identified and their growth kinetics studied. In order to further explore the influence of the newly generated intermetallic compounds on the laminated materials, their micromechanical properties were characterized. Interface performance

**Table 3** Theoretical density and calculated density of samples for different heating time

Heating time (h)	2	4	6	8	12	16
(g/cm <sup>3</sup> )	5.2860	5.1727	5.1400	5.1201	5.1187	5.0938
(g)	6.0	6.5	5.2	5.4	3.0	6.9
m <sub>water</sub> (g)	4.8600	5.2400	2.1800	4.3400	2.4100	5.5400
(g/cm <sup>3</sup> )	5.2632	5.1587	5.0980	5.0943	5.0847	5.0735

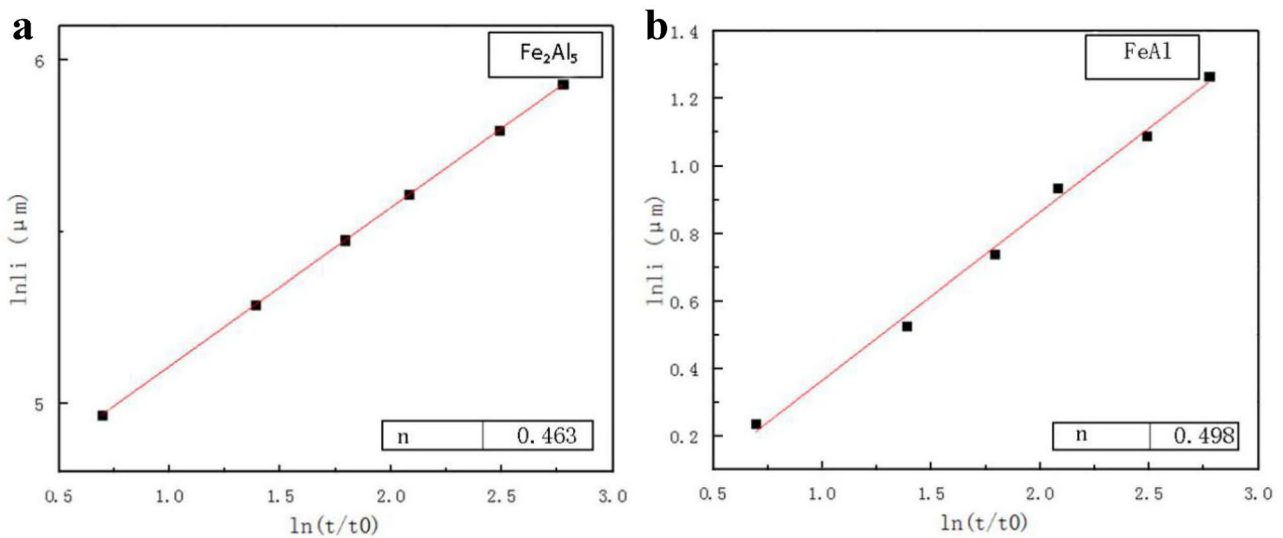


**Fig. 7** Thickness-heating time relationship and linear regression results of  $\text{Fe}_2\text{Al}_5$  and FeAl phases, respectively (**a**  $\text{Fe}_2\text{Al}_5$ , **b** FeAl)

is closely related to the microscopic structure of the interface. Therefore, in order to analyze the interface properties after diffusion, the microhardness near the interface of the intermetallic layer was determined. The microhardness of MIL composites after 2 h and 16 h of reaction is shown in Fig. 8. The microhardness of  $\text{Fe}_2\text{Al}_5$  phase was  $\sim 1000$  HV, the microhardness of carbon steel on both sides was 150 HV or greater. The microhardness of  $\text{Fe}_2\text{Al}_5$  phase in the literature [26] was suggested to be 1000 HV, which is consistent with this study. The microhardness distribution (Fig. 8) was as expected. Compared with stainless steel, carbon steel had very low Cr content, so in the vicinity of the centerline region, Cr-containing  $\text{Cr}_2\text{Al}_{13}$  phase was not formed, and between adjacent carbon steel was mainly hard  $\text{Fe}_2\text{Al}_5$  phase, which can be considered to uniform layer. The uniform layer is hard and brittle, so there were small cracks in the vicinity of diamond microhardness indentation in the uniform layer, as shown in Fig. 8c. The microhardness distribution near the interface after 16 h of carbon steel/Al reaction is shown in Fig. 8d, and the microhardness distribution trend is essentially identical to Fig. 8e. However, the microhardness at the interface was 863 HV, which is because of the formation of Fe-rich phase FeAl with B2 structure. There were no cracks

or evidence of delamination in the indented interface area, as shown in Fig. 8f. This indicates a good combination strength of two layers with a third ductile phase. It is obvious that the B2 layer can reduce the stress concentration at the interface and suppresses the crack growth. At the same time, the two are also closely combined by B2 layer to reduce the stratification effect in the multi-layer system.

### 3.5 Quasi-static compression ( $\sigma$ - $\epsilon$ curve) and fracture morphology

The special structure of the MIL composite is envisaged to have superior properties. At identical strain, the stress perpendicular to the laminar direction was greater than the stress parallel to the laminar direction [27]. Therefore, the compression performance perpendicular to the layered direction was studied. Stress-strain curve of carbon steel/Al after reaction for 4, 6, 12, and 16 h is presented in Fig. 9. The compression  $\sigma$ - $\epsilon$  curve of MIL composite after 4 and 16 h only had elastic deformation region and failure occurred at the end of the elastic deformation stage. That is, the sample broke almost immediately after the end of elastic region and no plastic deformation occurred. When Al was completely extruded, it entered the next stage. With the extension of reaction time, the FeAl phase generated gradually increased, so two different peaks appeared at hours 12 and 16. According to the microstructural analysis of the laminated composite, two peaks can be considered to be governed by two different phases,  $\text{Fe}_2\text{Al}_5$  and FeAl phases in MIL composites. FeAl intermetallic material has low density, high specific strength, good oxidation resistance, good corrosion resistance, and high-temperature friction and wear resistance. Compared with  $\text{Fe}_2\text{Al}_5$  uniform layer, FeAl provides better toughness

**Table 4** Fitted equation of thickness and time of intermetallic compound layer

Intermetallic phase	Kinetic index	Log of the reaction rate
$\text{Fe}_2\text{Al}_5$	0.463	4.646
FeAl	0.498	-0.133



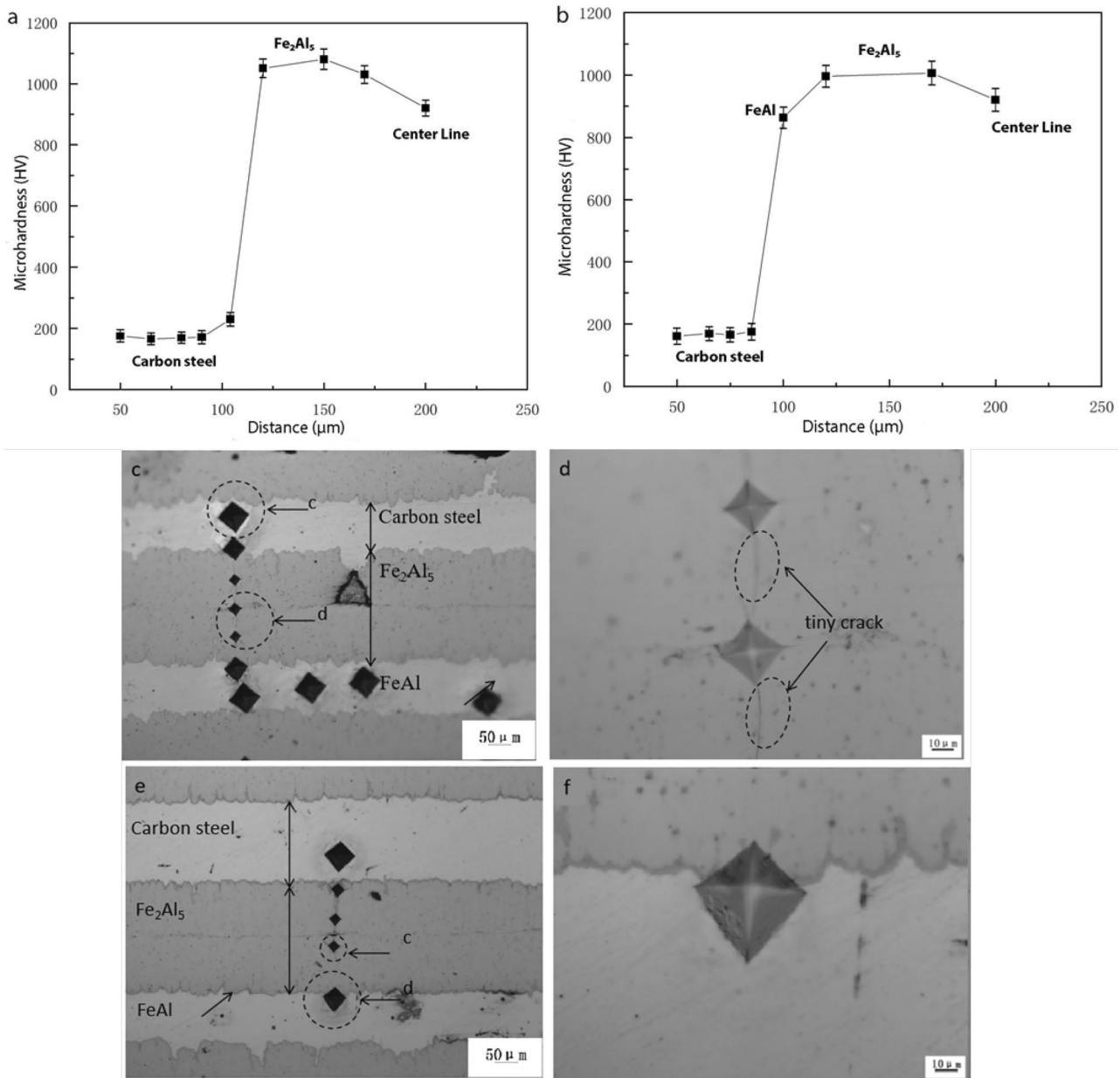


**Fig. 8** Microhardness distribution for different treatment (**a** microhardness curve heated for 2 h, **b, c** microhardness diagram heated for 2 h, **d** microhardness curve heated for 16 h, **e, f** microhardness diagram heated for 16 h)

[28]. In view of the existence of FeAl layer between the uniform layer and carbon steel, the complex tongue-like morphology of FeAl layer was weakened. Therefore, when the interlayer layer with toughness and toughness is destroyed, part of the crack propagation energy is dissipated. The FeAl layer reduces the interfacial stress concentration, inhibits crack growth, and reduces the delamination effect in the multilayer system. Since the MIL material forms an alternating stack of carbon steel and intermetallic compounds at the end of the reaction, cracks will break layer by layer when pressure is applied. That is, the crack forms the first peak in the

Fe<sub>2</sub>Al<sub>5</sub> layer and then passes through the Fe<sub>2</sub>Al<sub>5</sub> layer. The crack extends to the intermetallic compound FeAl layer and forms the second peak. Therefore, there are two peaks in the stress/strain curve. Table 5 lists values of the compressive strength and failure strain of all the tested samples.

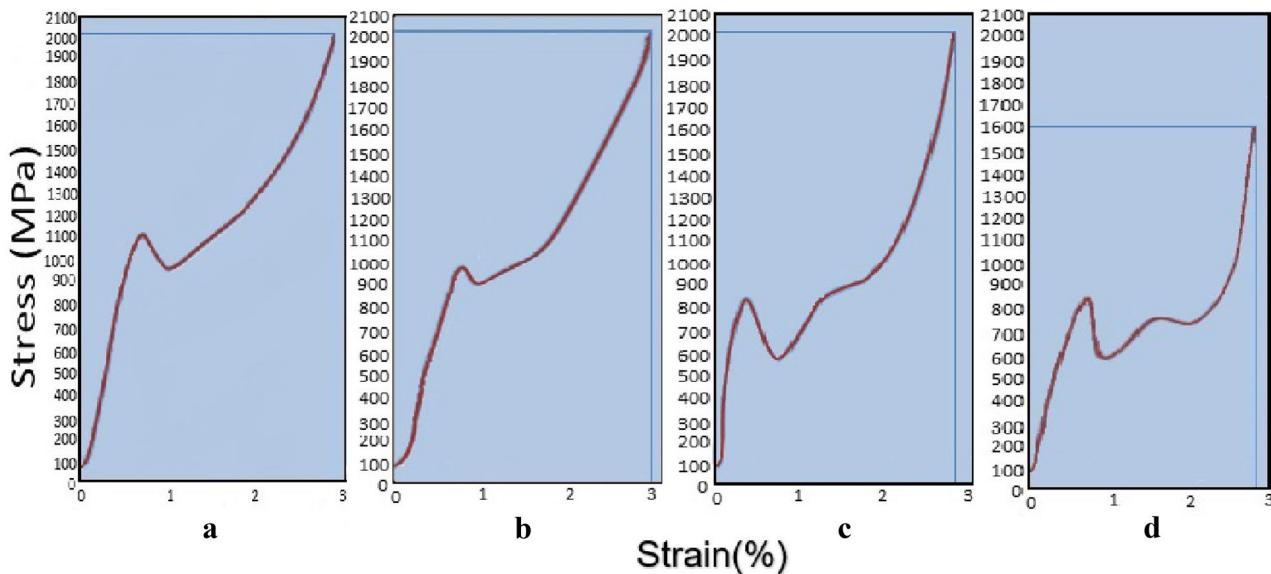
It can be seen from Table 5 that with the increase of reaction time, the FeAl phase increases, and the stress decreases after reaching the maximum value. However, with the increase of reaction time, FeAl phase increases and strain increases, which can absorb more energy, increase plasticity, and prevent brittle fracture.

**Table 5** Compressive strength and failure strain of carbon steel/Al reaction at 4, 6, 12, and 16 h

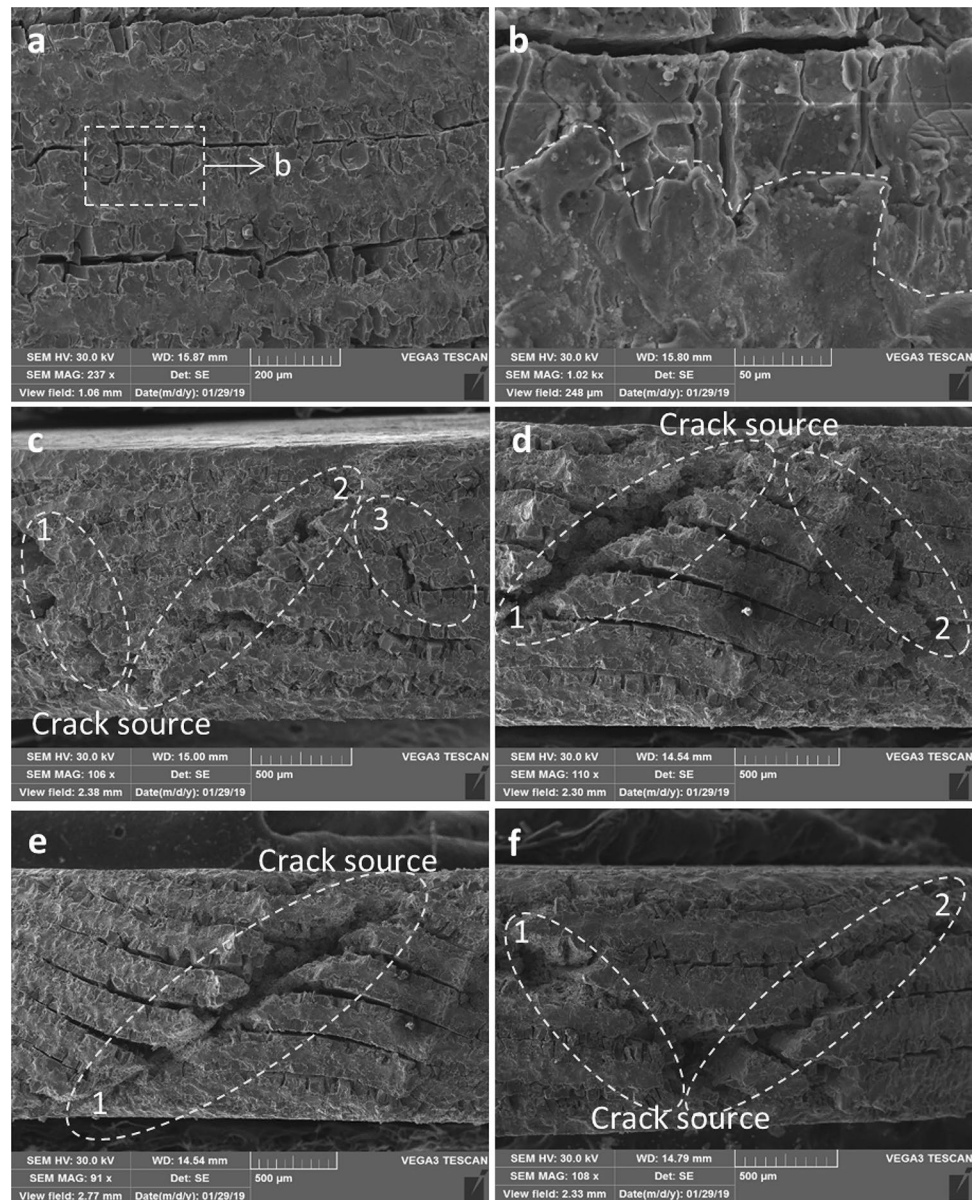
Time/h		Compressive strength/MPa	Failure strain/%
4		912	4.1
6		950	7.6
12	First peak	850	8.1
	Second peak	895	9
16	First peak	868	7.1
	Second peak	810	6.6

In order to further analyze the specific failure mode, the microfracture morphology of the materials after deformation was observed. Quasi-static compression specimens experienced both axial and radial deformation because of the partial fracture of the brittle uniform layer and plastic deformation of the ductile carbon steel. In view of energy dissipation combined with the deflection mechanism of the crack, the MIL composites did not undergo macroscopic fracture. The fracture morphology of the MIL composites is shown in Fig. 10. Figure 10a–c is the fracture morphology of the MIL composite after 4 h of reaction. It may be noted that the MIL composite cracked at the intermetallic centerline, forming a stratification phenomenon. However, there were also local areas that cracked. It can be seen from Fig. 10b that the micro-cracks perpendicular to the intermediate line were generated, and  $\text{Fe}_2\text{Al}_5$  phase ruptured, leaving voids. Since the B2 layer was present between the uniform layer and the carbon steel,

with complex tongue-like morphology of the uniform layer, the interface between the two did not undergo any cracking. It can be seen from Fig. 10c from the crack source that the two main cracks, 1 and 2, propagated in two  $45^\circ$  directions of the sample. Main crack 2 along the intermetallic centerline produced a secondary crack 3, which absorbed part of the crack growth energy until the crack reached the carbon steel layer, the secondary crack was stopped, and its growth also stopped. In addition, closer to the crack source, more severe cracking of the intermetallic centerline and the deformation of the carbon steel was observed, and the carbon steel was bent in the direction opposite to the crack source. Taking the main crack 1 of Fig. 10e as an example, in the direction in which the main crack 1 grew, the tough and ductile bonded sandwich structure layers were broken, and a part of the energy of crack propagation was dissipated. When the main crack 1 grew, a weak intermetallic centerline was encountered, and lateral micro-cracks extended along the intermediate line until another part of the energy of the crack propagation was consumed, and then, the lateral micro-crack stopped growing. The crack propagation after 16 h was similar. It can be clearly seen from Fig. 10 that the cracks of the samples with short reaction time are mostly in vertical direction and correspond to brittle fracture. While, with the increase of reaction time, FeAl phase increases, majority of the cracks in the sample were along the  $45^\circ$  direction, belonging to ductile fracture. In subsequent studies, the structure of the MIL composites was further analyzed to study the influence of material structure on compression performance.

**Fig. 9** Quasi-static compression curve of carbon steel/Al laminate after reaction for 4 (a), 6 (b), 12 (c), and 16 h (d)

**Fig. 10** Fracture morphology of quasi-static compression test of carbon steel/Al laminate after reaction for 4 (a–c), 12 (d, e), and 16 h (f)



## 4 Discussion

According to the Fe–Al binary phase diagram and previous studies [20–22], when the carbon steel reacts with Al at  $T=655\text{ }^{\circ}\text{C}$  and  $P=3.8\text{ MPa}$ , a  $\text{Fe}_2\text{Al}_5$  phase with a tongue-like morphology is present at the interface. In the present studies, as the reaction time progresses,  $\text{Fe}_2\text{Al}_5$  phase is rapidly transformed ( $\text{Fe}_2\text{Al}_5 \rightarrow \text{FeAl}$ ) during the cooling process. These phase transformation sequences are analyzed below:

First,  $\text{Fe}_2\text{Al}_5$  phase was formed at carbon steel/Al interface. When carbon steel was in contact with solid Al, atomic interdiffusion and interfacial reaction occurred to form an interfacial diffusion layer composed of a Fe–Al intermetallic. The generation of the interface is governed by thermodynamics

and kinetics. Both thermodynamic driving force and diffusion rate determine the chemistry of the interface. From the thermodynamic point of view, the most easily formed Fe–Al intermetallic is  $\text{FeAl}_3$  phase, but from the kinetic point of view, the growth kinetic coefficient of  $\text{Fe}_2\text{Al}_5$  phase is significantly larger than  $\text{FeAl}_3$  phase. At the same temperature, the growth rate of  $\text{Fe}_2\text{Al}_5$  phase is greater than  $\text{FeAl}_3$  phase [28]. At longer time, interdiffusion reactions occur, and the growth rate has a certain relationship with the melting point. At a constant temperature, the interdiffusion coefficient of the lower melting temperature intermetallic may be larger than the interdiffusion coefficient of intermetallic with high melting temperature. Furthermore, the growth rate of intermetallic with a larger interdiffusion coefficient is greater than the growth rate of the intermetallic with a small interdiffusion coefficient.

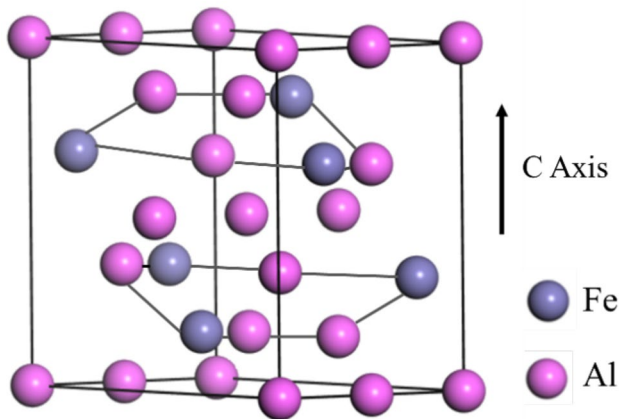


**Fig. 11** Folding model of  $\text{Fe}_2\text{Al}_5$

Thus, the intermetallic with lower melting point grows faster than one with a higher melting point. In the Fe-Al binary alloy system, the melting points of  $\text{Fe}_2\text{Al}_5$ ,  $\text{FeAl}_3$ ,  $\text{FeAl}_2$ , and FeAl phases are 1442, 1433, 1433, and 1583 K (1169, 1160, 1160, and 1310 °C), respectively. The melting point of  $\text{Fe}_2\text{Al}_5$  phase is relatively low, so its coefficient of mutual diffusion is larger. The reaction preferentially generates orthorhombic  $\text{Fe}_2\text{Al}_5$  phase at 655 °C.

From the  $\text{Fe}_2\text{Al}_5$  stacking model shown in Fig. 11, it can be seen that there are two C axis in the crystal structure, and the lattice nodes along the C axis are occupied only by Al atoms. Given that the atomic radii of Fe and Al are similar and 30% vacancies on the C axis, the Al atoms diffuse through the lattice of  $\text{Fe}_2\text{Al}_5$  at a higher rate to form  $\text{Fe}_2\text{Al}_5$  with tongue-like structure. A portion of the tongue-like structure extends inside the carbon steel, but majority of it is deposited on the carbon steel substrate, i.e., occupying the position of Al before the reaction. When the Al atoms diffuse to carbon steel side, the Fe atoms diffuse toward Al side, and the formation of the diffusion layer is a result of bidirectional diffusion of iron and aluminum.

The formation of  $\text{Fe}_2\text{Al}_5$  phase is completed in a short time, which is about a few minutes. In this study,  $\text{Fe}_2\text{Al}_5$  phase was also rapidly formed in the first few minutes of the reaction. Since the main phase of carbon steel is BCC ferrite, compared with austenitic stainless steel with FCC structure, the density is different, which is more conducive to the diffusion of atoms, so the  $\text{Fe}_2\text{Al}_5$  intermetallic compound layer is expected to grow faster in carbon steel.

## 5 Conclusions

1. The MIL composites prepared by reacting carbon steel/Al at 655 °C. The resulting intermetallics were  $\text{Fe}_2\text{Al}_5$  and FeAl, and  $\text{Fe}_2\text{Al}_5$  as the main phase. When the heat-

ing time was increased, the thickness of the FeAl intermetallic compound was gradually increased.

2. The thickness of  $\text{Fe}_2\text{Al}_5$  and FeAl layers was proportional to the square root of the holding time. The growth of  $\text{Fe}_2\text{Al}_5$  phase and FeAl phase with time followed parabolic relationship. The growth of both the phases was controlled by bulk diffusion.
3. The MIL composite obtained by the reaction was dense. The microhardness of  $\text{Fe}_2\text{Al}_5$  was ~1000 HV, and the microhardness of carbon steel was ~150 HV. The thin FeAl toughness layer between carbon steel and  $\text{Fe}_2\text{Al}_5$  can buffer the interface microhardness between high microhardness  $\text{Fe}_2\text{Al}_5$  and carbon steel with relatively low microhardness, and thereby reduces the stress concentration at the interface of the material and reduces delamination.
4. The compressive strength of laminated composites approached ~810–950 MPa, and the static compression performance of MIL materials heated for 16 h was the best. The sample after static compression fractured locally and did not break completely; axial and radial deformation occurred. The carbon steel layer experienced ductile fracture, and the uniform layer experienced brittle fracture demonstrating a mixed fracture condition.
5. The phase formation sequences in the carbon steel/Al reaction are shown as: complete transformation rapidly occurred and followed the sequence ( $\text{Fe}_2\text{Al}_5 \rightarrow \text{FeAl}$ ).

**Author contribution** Yu Wang: conceptualization, methodology, writing—review & editing. Y.X. Liu.: data curation, writing-original draft preparation. J.B. Hou: visualization, investigation. H.Y. Pan: resources, data curation. H.K. Mao: investigation. B. Liu: software, validation. P.K. Bai: supervision. H. Xu: supervision. R. D. K. Misra: writing—reviewing and editing.

**Funding** This research work was financially funded by the Key Research and Development Program of Shanxi Province (No. 201903D421080), Natural Science Foundation of Shanxi Province (No. 201801D221148), Stable Support Foundation of State Administration of Science Technology and Industry for National Defense (JB11-12), and The Key Research and Development Program of Anhui Province (Grant No.202004A05020070).

## Declarations

**Conflict of interest** The authors declare no competing interests.

## References

1. Fan W, Shan C, Guo H et al (2019) Dual-gradient enabled ultrafast biomimetic snapping of hydrogel materials [J]. *Sci Adv* 5(4):7174
2. Xie P, Liu Y, Feng M et al (2021) Hierarchically porous Co/C nanocomposites for ultralight high-performance microwave

- absorption. [J] *Advanced Composites and Hybrid Materials* 4:173–185
3. Rao V, Soboyejo O, Ritchie O (1992) Ductile-phase toughening and fatigue-crack growth in Nb-reinforced molybdenum disilicide intermetallic composites[J]. *Metall Trans A (Physical Metallurgy and Materials, Science)* 23(8):2249–2257
  4. Srivastava C, Singh T, Chowdhury G et al (2012) Microstructural characteristics of accumulative roll-bonded Ni–Al-based metal–intermetallic laminate composite[J]. *J Mater Eng Perform* 21(9):1912–1918
  5. Rohatgi A, Harach J, Vecchio S et al (2003) Resistance-curve and fracture behavior of Ti–Al<sub>3</sub>Ti metallic–intermetallic laminate (MIL) composites[J]. *Acta Mater* 51(10):2933–2957
  6. Wu H, Mu Z, Qi G et al (2021) Negative permittivity behavior in Ti<sub>3</sub>AlC<sub>2</sub>-polyimide composites and the regulation mechanism[J]. *J Mater Sci Mater Electron* 32:10388–10397
  7. Vecchio S (2003) Synthetic Multi-functional materials by design using metallic–intermetallic laminate (MIL) composites[J]. *Nano and Microstructural Design of Advanced Materials* 243–254
  8. Lazurenko D, Mali V, Thoemmes A (2015) Formation of metal–intermetallic laminate composites by spark plasma sintering of metal plates and powder work pieces[J]. *Appl Mech Mater* 698(698):277–282
  9. Bataev IA, Bataev AA, Mali VI et al (2012) Structural and mechanical properties of metallic–intermetallic laminate composites produced by explosive welding and annealing[J]. *Mater Des* 35:225–234
  10. Lazurenko V, Bataev A, Mali I et al (2018) Synthesis of metal–intermetallic laminate (MIL) composites with modified Al<sub>3</sub>Ti structure and in situ synchrotron X-ray diffraction analysis of sintering process[J]. *Mater Des* S0264127518303083
  11. Assari H, Eghbali B (2019) Solid state diffusion bonding characteristics at the interfaces of Ti and Al layers[J]. *J Alloys Compd* 773:50–58
  12. Yuan N, Li L, Wang J (2018) Study of the microstructure modulation and phase formation of Ti Al<sub>3</sub>Ti laminated composites[J]. *Vacuum* 157:481–486
  13. Lv Y, Sun B, Li D, Xiao L, Ma L (2018) Effect of layer sequence on the mechanical properties of Ti/TiAl laminates[J]. *Mater Des* 143:160–168
  14. Azimi M, Toroghinejad Reza, Shamanian M (2017) The Effect of Strain on the Formation of an Intermetallic Layer in an Al–Ni Laminated Composite[J]. *Metals* 445(7):1–14
  15. Yener T, Yener C, Zeytyn S (2016) Electromagnetic-shielding effectiveness and fracture behavior of laminated (Ni–NiAl<sub>3</sub>) composites[J]. *Mater Technol* 50(6):899–902
  16. Brunelli K, Peruzzo L, Dabalà M (2015) The effect of prolonged heat treatments on the microstructural evolution of Al/Ni intermetallic compounds in multi layered composites[J]. *Mater Chem Phys* 149:350–358
  17. Wang Y, Vecchio K (2016) Microstructure evolution in Fe-based-aluminide metallic–intermetallic laminate (MIL) composites. *Mater Sci Eng A* 649:325–337
  18. Cheng J, Wang J (2011) Study of microstructure and phase evolution of hot-dipped aluminide mild steel during high-temperature diffusion using electron backscatter diffraction [J]. *Appl Surf Sci* 257(10):4663–4668
  19. Glasbrenner H, Stein-fechner K, Konys J (2000) Scale structure of aluminised F82H-mod. steel after HIP treatment [J]. *Fusion Eng Des* 51:105–110
  20. Karfoul K, Tatlock J, Murray T (2007) The behaviour of iron and aluminium during the diffusion welding of carbon steel to aluminium[J]. *J Mater Sci* 42(14):5692–5699
  21. Rastkar R, Rezvani N (2015) The effects of processing time on the microstructure and composition of plasma pack-aluminized and oxidized Surface layers on low carbon Steel [J]. *Metall Mater Trans A* 46(9):4132–4142
  22. Cui L, Chen B, Chen L et al (2018) Dual beam laser keyhole welding of steel/aluminum lapped joints [J]. *J Mater Process Technol* S092401361830061X
  23. Bhupinder D, Brown W, Kulkarni N (2018) Effect of silicon, manganese and nickel present in iron on the intermetallic growth at iron - aluminum alloy interface[J]. *J Alloys Compd* 769:777–787
  24. Tanaka Y, Kajihara M, Watanabe Y (2007) Growth behavior of compound layers during reactive diffusion between solid Cu and liquid Al [J]. *Mater Sci Eng A* 445–446:355–363
  25. Bader S, Gust W, Hieber H (1995) Rapid formation of intermetallic compounds interdiffusion in the Cu Sn and Ni Sn systems. *Acta Metall Mater* 43(1):329–337
  26. Price D, Jiang F, Kulin M et al (2011) Effects of ductile phase volume fraction on the mechanical properties of Ti–Al<sub>3</sub>Ti metal–intermetallic laminate (MIL) composites [J]. *Mater Sci Eng A* 528(7–8):3134–3146
  27. Jiang T, Lv F, Zhang N et al (2014) Research status and development of Fe–Al intermetallics compounds/ceramics composites [J]. *Modern technical ceramics* 35(02):9–19
  28. Yin C, Zhao X, Liu X, Han W, Li Z (2013) Effect of Si on growth kinetics of intermetallic compounds during reaction between solid iron and molten aluminum[J]. *Trans Nonferrous Metals Soc China* 23(02): 556–561

**Publisher's Note** Springer Nature remains neutral with regard to jurisdictional claims in published maps and institutional affiliations.